Observation of warm, higher energy electrons transiting a double layer in a helicon plasma

Yung-Ta Sung,[a] Yan Li, and John E. Scharer
Department of Electrical and Computer Engineering, University of Wisconsin-Madison, 1415 Engineering Drive, Madison, Wisconsin 53706, USA

(Received 16 December 2014; accepted 9 March 2015; published online 25 March 2015)

Measurements of an inductive RF helicon argon plasma double layer with two temperature electron distributions including a fast (>80 eV) tail are observed at 0.17 mTorr Ar pressure. The fast, untrapped electrons observed downstream of the double layer have a higher temperature (13 eV) than the trapped ($T_e = 4$ eV) electrons. The reduction of plasma potential and density observed in the double layer region would require an upstream temperature ten times the measured 4 eV if occurring via Boltzmann ambipolar expansion. The experimental observation in Madison helicon experiment indicates that fast electrons with substantial density fractions can be created at low helicon operating pressures. © *2015 AIP Publishing LLC*.
[http://dx.doi.org/10.1063/1.4916051]

In our previous research on Madison Helicon eXperiment (MadHeX),[1,2] we have observed plasma self-bias double layer effects at lower densities (10^{8-9} cm^{-3}) with ion beams corresponding to plasma potential double layers in the capacitive coupling discharge regime. This lower density capacitive regime[3] corresponds to RF skin depths comparable to or larger than the 10 cm diameter column. The magnitude of ion beam acceleration in the previous capacitively coupled experiments on MadHeX is much larger than typical inductive discharges and occurs over larger spatial dimensions, about 13–100 Debye lengths. In the previous MadHeX measurements of the scaling of the beam energy in the lower density capacitive coupling mode plasma, we showed by examining the electron and ion plasma frequencies relative to the RF that the large ion energies are a result of the plasma self-biasing effect.[1,2] Under large RF-timescale axial fluctuations in the plasma potential, electrons are expelled from the source region, while the heavier ions do not respond to the high frequency oscillations. The plasma self-bias effect in the capacitive RF coupling regime was exploited to allow ion acceleration to much higher energies than by ambipolar expansion.[4]

Takahashi *et al.*[5] have observed a current-free double layer in their Chi-Kung system in the inductive regime. Higher and lower electron temperatures were observed upstream and downstream of the double layer, respectively. Cohen *et al.*[6] have reported ion acceleration of 30 to 65 eV in their Magnetic Nozzle eXperiment (MNX) helicon device with a magnetic nozzle in the inductive coupling regime. They concluded that the ion acceleration is not due to plasma Boltzmann expansion,[4] nor magnetic nozzle acceleration. They conclude that a double layer formed near the aperture between source and diffusion chambers primarily causes the ion acceleration. Evidence of a two-temperature electron distribution, with a higher temperature (6–20 eV), small density tail (0.1%) electron temperature, was also measured downstream of the double layer.

We report on MadHeX experiments operating in a higher density (10^{10-11} cm^{-3}), low pressure (0.17 mTorr), inductively coupled RF (900 W net power coupled) mode. We observe two-temperature electron distributions with a moderate density of 3×10^{10} cm^{-3} (1/15 the upstream density) downstream of the double layer with a hotter temperature (4 times the measured upstream bulk T_e).

The MadHeX (see Figure 1) consists of an upstream double half-turn helix antenna RF source, a magnetic nozzle, and a downstream magnetic expansion chamber. The Pyrex source chamber is a 120 cm long tube with a 10 cm inner-diameter (ID) dimension. An 18 cm long × 13 cm diameter antenna with an electrically grounded external steel mesh screening (18 cm ID) surrounds the chamber with the downstream edge of the antenna denoting the $z = 0$ cm position. The expansion chamber is made of stainless steel, which is 70 cm in length with a 45 cm diameter. An 8-in. Varian turbo-molecular pump is connected at the bottom of the expansion chamber. With the operation of a diaphragm mechanical pump joined to the turbo pump, typical base pressures for MadHeX are less than 3×10^{-6} Torr.

The Pyrex tube is centered inside six water-cooled electromagnetic coils. Each is 7 cm wide with an 18 cm bore. A Sorensen DC power supply provides up to 180 A, which corresponds to a magnetic field up to 1.04 kG in the source region with a magnetic nozzle ($R = 1.44$) located at $z = 28$ cm. RF power is provided by an HP 33120A function generator, which is fed to a Comdel CX10KS amplifier, which can deliver up to 10 kW steady-state RF power. A two-capacitor matching network is used to match the plasma loaded antenna impedance to the RF generator. Both forward and reflected powers are measured with a Connecticut Microwave directional coupler with calibrated RF diodes.

For the current experimental conditions, an axial magnetic field of 340 G in the RF source region is produced by the solenoid magnets. The net coupled 900 W RF power,

[a]Electronic mail: ysung2@wisc.edu

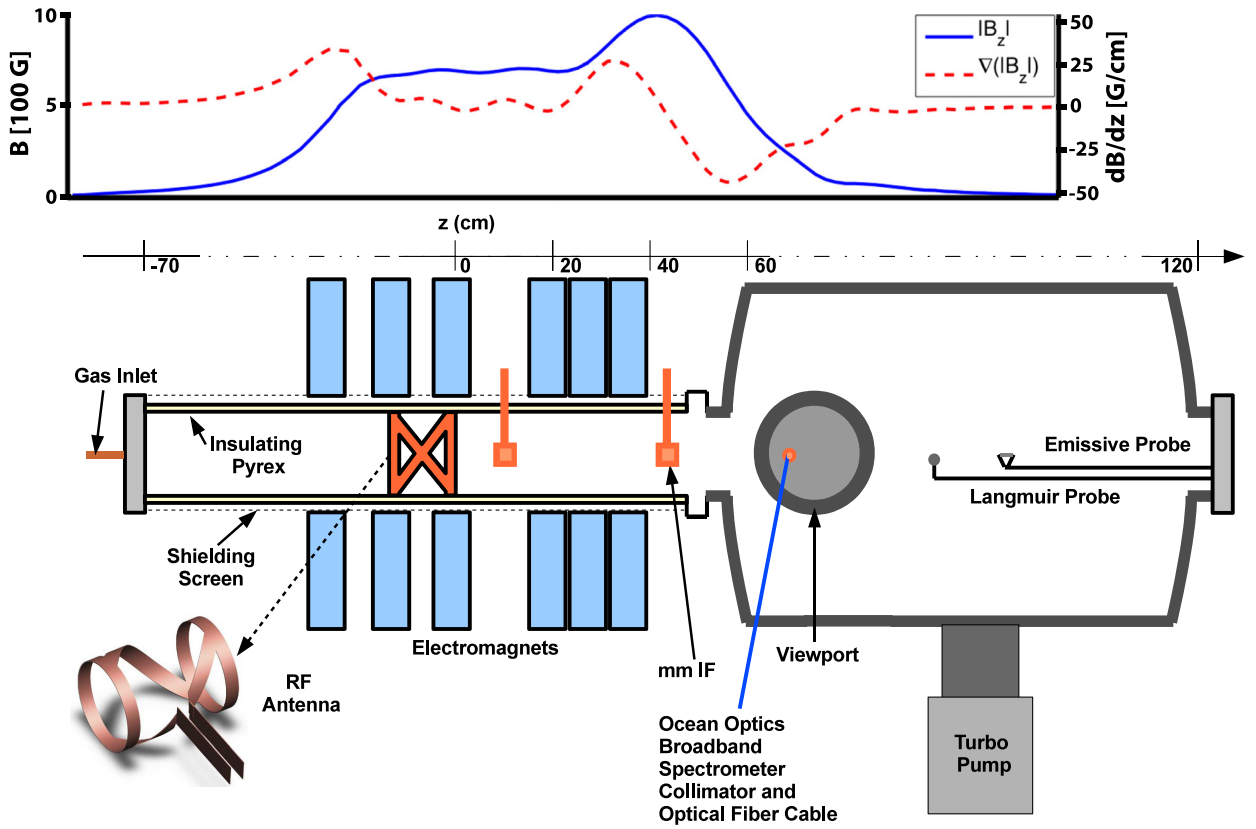

FIG. 1. MadHeX. The static magnetic field value (units in Gauss) and gradient (units in Gauss/cm) are shown above the system. The diagnostics tools are shown within MadHeX.

taking account of small reflections, is applied for our MadHeX operating conditions to the plasma through the antenna at 13.56 MHz via the matching network. Argon gas flows at 2 sccm into the experiment through a copper tube (5 mm ID) attached to an upstream aluminum end plate where the pressure is 0.58 mTorr. This corresponds to a pressure of 0.17 mTorr measured at the junction between the Pyrex tube and the large expansion chamber ($z = 52$ cm) where the plasma double layer is observed.

The Atomic Data and Analysis Structure (ADAS)[7–9] is a computational code developed to model radiation from ions for a variety of atomic species. The ADAS Collisional-Radiative (CR) model consists of a set of coupled differential equations for corresponding 35 level parents. These parents are groupings of excited states of singly ionized argon (Ar II) that has the same electron configuration but differs in their total angular momentum. The Maxwellian electron temperature (T_e) can be determined with data computed via using the model for argon ions if the plasma density is known. The code used here does not solve the coupled differential equations but relies on pre-calculated values and tables. Interpolation is used to find the population rates for the plasma density (obtained by mm wave interferometer (IF)[10,11] and an RF filtered[1] Langmuir probe (LP)) and determines the electron temperature that lies between pre-calculated values provided, $1 \times 10^{10}\,\mathrm{cm}^{-3} \le n_e \le 2 \times 10^{12}\,\mathrm{cm}^{-3}$ and $0.5\,\mathrm{eV} \le T_e \le 500\,\mathrm{eV}$. A calibrated Ocean Optics ST2000 spectrometer and a spectrum preprocess Matlab code are used to measure the population densities of the excited states, which are an input to the ADAS CR code.

A planar disc ($d = 2.4$ mm) single Langmuir probe whose face is oriented perpendicular to the magnetic field is used to measure the electron temperature and density. In the present work, Langmuir and emissive probe potential fluctuations measured in our inductively coupling mode[3] plasma are much lower than the previous capacitively coupled RF plasma modes. A resonant RF filter[1] is used to increase the probe impedance at the RF driving frequency to reduce oscillations that can affect electron temperature measurements.[12]

Electron temperatures are determined from the observed I-V Langmuir probe traces near the floating potential using a straight-line fitting to the logarithmic electron current (measured current with ion current subtracted). In the presence of larger fluctuations of the plasma potential, the farthest-negative edge of the I-V traces is used for electron temperature fitting.[12] The ion density is calculated from the ion saturation current by fitting the ion saturation region (measured from −40 to −75 V) of the I-V traces, subtracting the linear increase from sheath expansion, and using the formula[13]

$$n_e = \frac{I_{sat}}{0.6eA\sqrt{\frac{T_e}{M_{Ar}}}}, \tag{1}$$

where I_{sat} is the ion saturation current, e is the elemental charge, A is the probe area, T_e is the electron temperature, and M_{Ar} is the argon ion mass. The ADAS code, LP, and mm wave IF diagnostics used to determine electron temperatures and densities are found to be in good agreement providing support for the techniques used.

The emissive probe consists of a 25 μm diameter, 6.8 mm long tungsten filament spot-welded between two gold-plated nickel wires. The nickel wires are then ceramic-coated. A circuit that consists of a 6 V battery and a 10 Ω resistor is used to heat the probe filament. The emissive probe operated here is swept and biased with respect to chamber ground via a custom supply based on the PA241 operational amplifier. The plasma potential is measured using the inflection point method.[14]

The line-average electron density (n_e) in the 10 cm diameter Pyrex chamber is determined by our 105 GHz Mach-Zehnder mm wave interferometer. The wave propagation is nearly identical to O-mode propagation in the regimes where the interferometer is operated. The phase shift varies linearly with the electron density, given that

$$n_e = \frac{2.07 f \Delta\phi}{d}\ \mathrm{cm}^{-3}, \tag{2}$$

where f is the interferometer frequency in Hz, d is the chamber plasma diameter in cm, and $\Delta\phi$ is the phase shift in degrees.[9]

The axial dependence of the plasma potential, electron temperature, and electron density was examined for the inductively coupled RF, low pressure plasmas. The plasma parameters shown in Figures 2(b) and 2(c) are averaged values (from 5 measurements). The uncertainties in the electron number density, temperature, and plasma potential are ±20%, ±10%, and ±10%, respectively. Figure 2(a) indicates the axial magnetic field and field line distribution vs. z (10–80 cm) for a magnet current of I = 60 A that yields a 340 G field in the antenna region. Figure 2(b) shows that the time-averaged plasma potential (relative to the expansion chamber ground) varies from 90 V to 10 V as the emissive probe is moved axially from z = 40 cm to z = 80 cm, where z = 0 cm is the downstream edge of the 18 cm long antenna. The plasma potential drops rapidly in the double layer region from 90 V (at z = 52 cm) to 10 V (at z = 56 cm) and then gradually rises to 25 V (at z = 80 cm). Ionization of slow moving neutrals by fast electrons could influence this plasma potential rise of slower ions before reaching the grounded expansion chamber. Note in Figure 2(b) that the measured upstream plasma potential fluctuations are ±15% and are less than ±5% after the potential drop in the downstream region. The electron temperatures obtained by ADAS (given the density obtained by the mm wave IF) just upstream of the double layer and via the LP at lower densities downstream are shown in Figure 2(c).

A population of electrons with electron temperatures of 3.5–4 eV was observed in the upstream region (z < 50 cm), while much warmer electrons (T_e = 10–13 eV) were measured downstream of the double layer in the expansion chamber. The axial evolution of the Maxwellian electron temperature as measured by the Langmuir probe and ADAS diagnostics peaked at z = 50 cm (13 eV) and gradually decreased to 10 eV at z = 75 cm. The on-axis density measured with a single Langmuir probe decreases from $3.5 \times 10^{11}\,\mathrm{cm}^{-3}$ (z = 40 cm) to $1.5 \times 10^{10}\,\mathrm{cm}^{-3}$ (z = 70 cm). The density measured via interferometry indicates a line-average density of $2.8 \times 10^{11}\,\mathrm{cm}^{-3}$ at z = 42 cm and $3.6 \times 10^{10}\,\mathrm{cm}^{-3}$ at z = 12 cm. If a radial density peaking factor of 1.3 is assumed, the densities are $3.6 \times 10^{11}\,\mathrm{cm}^{-3}$ at z = 42 cm and $4.7 \times 10^{11}\,\mathrm{cm}^{-3}$ at z = 12 cm, respectively. The peak densities determined from the IF at z = 42 cm are comparable to the values determined by the on-axis Langmuir probe.

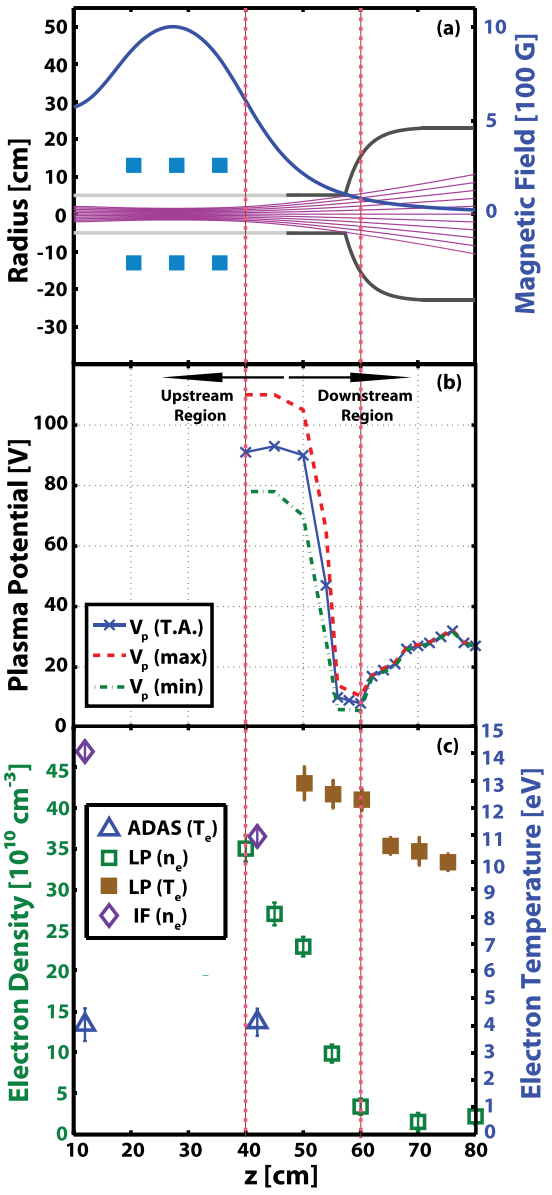

FIG. 2. (a) The static magnetic field value (dark blue line) and field lines (pink lines) as MadHeX are operated in a nozzle configuration with a magnetic field of 340 G in the antenna region. Blue solid squares indicate the positions of magnets. (b) The arrows indicate the upstream (z < 48 cm) and downstream (z > 48 cm) regions, respectively. The time-averaged value (blue line with x markers) and the upper and lower fluctuation limits (red and green dashed lines) of the plasma potential measured via a swept emissive probe for P_{RF} = 900 W, Q = 2 sccm, and B = 340 G. (c) The electron densities and temperatures are measured with LP, IF, and ADAS diagnostics. The purple diamonds and green squares are the measured density values from the IF and LP, respectively. The blue triangles and brown solid squares indicate the electron temperature obtained from the ADAS and LP diagnostics with the error bars indicating the variation in 5 separate measurements.

To maintain plasma quasi-neutrality, ambipolar (Boltzmann) expansion[4] is characterized by the balance

between an ambipolar electric field and the gradient in the electron pressure. The electron density and plasma potential are related through the Boltzmann relation as follows:

$$n_e(z) = n_{e0} \exp\left[\frac{e(V_p(z) - V_{p0})}{kT_e}\right], \quad (3)$$

where $n_e(z)$ and $V_p(z)$ are the local electron density and plasma potential, respectively, n_{e0} is the electron density at $z = 0$, V_{p0} is the plasma potential at $z = 0$, and T_e is the electron temperature. The potential profile can be predicted as a function of the electron density, given by

$$V_p(z) = V_{p0} + \frac{kT_e}{e} \ln\left[\frac{n_e(z)}{n_{e0}}\right]. \quad (4)$$

The implied Maxwellian electron temperature can be determined from a linear-fit to the resultant $n_e(z)/n_{e0}$ versus $(V_p(z) - V_{p0})$ plot. If the electron temperature fit matches the measured electron temperature, the plasma expansion is assumed to follow a Boltzmann relation.[15] For our current experimental measurements, the predicted electron temperature is 40 eV, which is substantially (10 times) higher than the measured upstream electron temperatures (3.5–4 eV). This indicates that the plasma density reduction through the double layer is not well explained by a Boltzmann relation.

In our previous publications,[1,2] we observed a self-biasing effect on MadHeX for a lower (100 W) RF power case. The large RF fluctuations of the plasma potential in the capacitive mode are responsible for the mechanism. For the current experimental conditions operating at higher (900 W) RF powers, $\omega_{pe}^2/\omega_{RF}^2 \approx 40\,000$, $\omega_{pi}^2/\omega_{RF}^2 \approx 0.60$, where ω_{RF}, ω_{pe}, and ω_{pi} are RF, electron and ion plasma frequencies, respectively. The electrons are still able to fully respond to the fluctuating instantaneous plasma potential profile and the ions can also respond to the time-dependent plasma potential fluctuations. The higher electron density ($2.8 \times 10^{11}\,\mathrm{cm}^{-3}$) also allows the plasma to better shield the electrostatic fields from RF antenna in the source region. Thus, we expect plasma self-bias effects to be active primarily during the lower density transient (10–100 μs) start-up phase when $\omega_{pe} \gg \omega_{RF} \gg \omega_{pi}$.

We have also measured the plasma potential variation upstream near the grounded end plate. The plasma potential drops in this region with a large (90%) portion of the magnetic flux and plasma terminating on the insulating Pyrex wall before reaching the end plate. Thus, the net electron currents are quite low and comparable to the current free floating upstream plate conditions we observed in the capacitive coupling regime.[1]

The mean-free-path for ion-neutral charge-exchange (CX) collisions can be calculated by

$$\lambda_{cx} = \frac{1}{n_g \sigma_{cx}}, \quad (5)$$

where $n_g = 3.3 \times 10^{11} p[\mathrm{mTorr}]$ and σ_{cx} is the total ion charge exchange collisional cross section, which is a function of the incident argon ion energy. For an 80 V ion, Phelps[16] finds a cross-section of $39.4 \times 10^{-16}\,\mathrm{cm}^2$. Given the operating pressure of 0.17 mTorr in the expansion chamber, $\lambda_{cx} = 77$ cm. For 10 eV electrons, the electron-Ar neutral cross section[16] is $\sigma_{en} = 15 \times 10^{-16}\,\mathrm{cm}^2$, which determines an electron-neutral mean-free-path of $\lambda_{en} = 122$ cm. Hence, over the 4 cm long double layer region of the expansion region, the plasma is electron- and ion-neutral collisionless. The upstream to downstream density drops by a factor of 15.

As shown as in Figure 2(b), the plasma potential begins to increase from the minimum by 25 V beyond $z = 60$ cm. This smaller increase in downstream potential could be due to plasma fast electron ionization of slower moving neutrals in the grounded expansion chamber. The fast electrons that pass over the double layer could ionize some of the argon neutrals creating slower ions in this region, which can cause the plasma potential to increase there.

For the plasma parameters shown in Figures 2(b) and 2(c), the spatial extent of the double layer is 4 cm. Assuming upstream plasma values of $T_e = 4$ eV and $n_e = 3 \times 10^{11}\,\mathrm{cm}^{-3}$, it corresponds to 1,500 Debye lengths, which is on the order of the spatial extent of other double layers[17,18] measured in expanding helicon plasmas.

In sum, we observe in the 900 W inductive plasma coupling regime with a magnetic nozzle a "collisionless" plasma double layer potential drop of 80 V with hotter ($T_{e,downstream} = 10$–13 eV), untrapped electron tail temperatures downstream than upstream ($T_{e,upstream} = 3.5$–4 eV). The presence of the two temperatures indicates that fast electrons with substantial density fractions can be created at low helicon operating pressures.

The authors would like to thank the University of Wisconsin-Madison for supporting this research.

[1]M. Wiebold, Y.-T. Sung, and J. E. Scharer, Phys. Plasmas **19**, 053503 (2012).
[2]M. Wiebold, Y.-T. Sung, and J. E. Scharer, Phys. Plasmas **18**(6), 063501 (2011).
[3]A. Degeling, N. Mikhelson, R. W. Boswell, and N. Sadeghi, Phys. Plasmas **5**, 572 (1998).
[4]W. Manheimer and R. Fernsler, IEEE Trans. Plasma Sci. **29**(1), 75–84 (2001).
[5]K. Takahashi, C. Charles, R. W. Boswell, T. Kanedo, and R. Hatakeyama, Phys. Plasmas **14**, 114503 (2007).
[6]S. Cohen, X. Sun, N. Ferraro, E. Scime, M. Miah, S. Stange, N. Siefert, and R. Boivin, IEEE Trans. Plasma Sci. **34**, 792 (2006).
[7]See http://www.adas.ac.uk/ for ADAS website.
[8]E. Sciamma, Ph.D. thesis, University of Texas at Austin, 2007.
[9]C. M. Denning, Ph.D. thesis, University of Wisconsin at Madison, 2008.
[10]K. Akhtar, J. E. Scharer, S. Tysk, and E. Kho, Rev. Sci. Instrum. **74**, 996 (2003).
[11]C. M. Denning, M. Wiebold, and J. Scharer, Phys. Plasmas **15**, 072115 (2008).
[12]L. Oksuz, F. Soberon, and A. R. Ellingboe, J. Appl. Phys. **99**(1), 013304 (2006).
[13]M. A. Lieberman and A. J. Lichtenberg, *Principles of Plasma Discharges and Materials Processing*, 2nd ed. (Wiley, Hoboken, New Jersey, 2005).
[14]J. R. Smith, N. Hershkowitz, and P. Coakley, Rev. Sci. Instrum. **50**, 210–218 (1979).
[15]M. D. West, C. Charles, and R. W. Boswell, J. Phys. D **42**(24), 245201 (2009).
[16]A. V. Phelps, J. Phys. Chem. Ref. Data **20**, 557 (1991).
[17]X. Sun, A. Keesee, C. Biloiu, E. Scime, A. Meige, C. Charles, and R. Boswell, Phys. Rev. Lett. **95**, 025004 (2005).
[18]E. E. Scime, I. A. Biloiu, J. J. Carr, S. C. Thakur, M. Galante, A. Hansen, S. Houshmandyar, A. M. Keesee, D. McCarren, S. Sears, C. Biloiu, and X. Sun, Phys. Plasmas **17**(5), 055701 (2010).